Available online at www.sciencedirect.com
ScienceDirect
Journal of Photochemistry and Photobiology A: Chemistry 190 (2007) 161–168
Journal of Photochemistry and Photobiology A:Chemistry
www.elsevier.com/locate/jphotochem

Nonadiabatic dissociation dynamics of Cl···HD van der Waals complex initiated by electron detachment of Cl^-–HD

Subhas Ghosal, Susanta Mahapatra *

School of Chemistry, University of Hyderabad, Hyderabad 500046, India

Received 23 November 2006; received in revised form 28 February 2007; accepted 2 March 2007
Available online 12 March 2007

Abstract

Nuclear dynamics following the electron detachment of the Cl^-–HD anion is investigated by a time-dependent wave packet propagation approach. Photodetachment of Cl^-–HD promotes it to the van der Waals well region of the reactive Cl···HD potential energy surface. The latter is a manifold of three electronic states coupled by the electronic and (relativistic) spin-orbit coupling. Among the three surfaces, the electronic ground one is of $^2\Sigma_{1/2}$ type and yields products in their electronic ground state. The remaining two, $^2\Pi_{3/2}$ and $^2\Pi_{1/2}$, on the other hand, yield products in their excited electronic states. However, these two can yield products in their electronic ground state via nonadiabatic transitions to the $^2\Sigma_{1/2}$ state. The channel specific, HCl + D or DCl + H or Cl + HD, dissociation probabilities on this latter state are calculated both in the uncoupled and coupled surface situations. Separate initial transitions (via, photodetachment) to the $^2\Sigma_{1/2}$, $^2\Pi_{3/2}$ and $^2\Pi_{1/2}$ adiabatic electronic states of Cl···HD are considered in order to elucidate the nonadiabatic coupling effects on this important class of chemical reactions initiated by an electron detachment.

Keywords: Nonadiabatic photodissociation dynamics; Van der Waals complex; Cl^-–HD; Cl···HD

1. Introduction

Molecular dissociation following photodetachment of its anionic precursor represents a rarely explored class of chemical reactions, particularly, when the latter are guided by nonadiabatic interactions. Anion photoelectron spectroscopy [1–3] by and large has been utilized to probe the bound vibronic level structure of the corresponding neutral species, however, the dissociation of the latter can become an important event when its equilibrium geometry differs significantly from that of the anion precursor. More specifically, if the 'transition state' or the repulsive region of the potential energy surface (PES) of the neutral species is probed by photodetachment [1]. Experimental measurement of such a process is also tedious and it requires a careful combination of the photoelectron spectroscopy with the photofragment translational spectroscopy. Such a combination allows to record the kinetic energies and recoil angles of the photoelectron and the final photofragments are measured in co-incidence [3]. This technique has been applied to study the dissociative photodetachment dynamics of weekly bound cluster anions [4] and van der Waals complexes [5].

Over the past years the $Cl + H_2$ reactive system has been extensively studied both theoretically and experimentally [6]. Experimental photodetachment measurements have probed the van der Waals well of the reagent asymptote of the reactive $Cl + H_2$ (HD) PES [7]. This has been corroborated by the theoretical studies for the first time from our group [8,9]. Now, since the photodetachment of the anion precursor in this case samples the reagent channel of the reactive PES of the neutral, the repulsive energy in the latter may be sufficient to trigger chemical reactions.

The dissociation of Cl···HD followed by photodetachment of $C1^-$–HD is examined in this paper. The low-lying PESs of neutral Cl···HD are coupled by electronic and relativistic spin-orbit (SO) coupling [10,11]. The ground electronic state of Cl···HD is of $^2\Sigma_{1/2}$ type and the two immediate next excited electronic states are of $^2\Pi_{3/2}$ and $^2\Pi_{1/2}$ type in the collinear arrangements of the three nuclei ($1^2A'$, $1^2A''$ and $2^2A'$ symmetries, respectively, in non-collinear geometries). Of these only the lower state of A' symmetry ($^2\Sigma_{1/2}$) correlates with the electronic ground state of the products HCl/DCl ($X^1\Sigma^+$) + H (^2S), whereas, the other two excited states (the components

* Corresponding author. Fax: +91 40 23011537.
E-mail address: smsc@uohyd.ernet.in (S. Mahapatra).

1010-6030/$ – see front matter © 2007 Elsevier B.V. All rights reserved.
doi:10.1016/j.jphotochem.2007.03.001

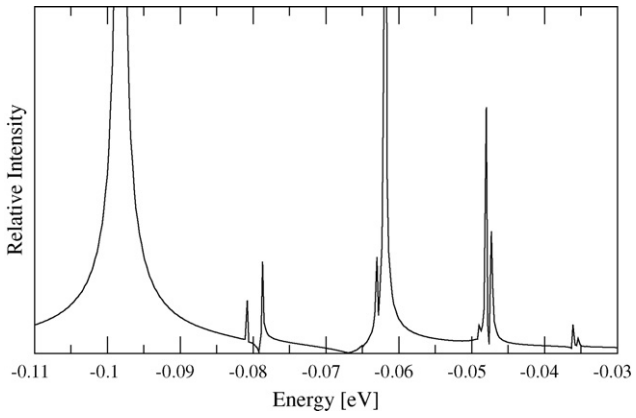

Fig. 1. The bound energy level spectrum of the electronic ground state of the Cl^-–HD anion obtained by spectral quantization method and locating a stationary GWP near the equlibrium geometry of Cl–HD (at $R \sim 6.01a_0$, $r \sim 1.402a_0$ and $\gamma \sim 0^\circ$ with width parameters 0.25, 0.25 and $0.2a_0$ along these coordinates, respectively). The intensity in arbitary units is plotted as a function of the energy measured relative to that of equilibrium geometry of the electronic ground state of Cl^-–HD.

of the $^2\Pi$ state) correlate with the products in their electronic excited state, HCl/DCl ($^3\Pi$) + H(^{2}S) (e.g. see Fig. 1 of Ref. [9]). The product excited state is considerably high in energy, thus the $^2\Pi_{3/2}$ and $^2\Pi_{1/2}$ states remain non-reactive in the adiabatic Born–Oppenheimer picture for low and moderate collision energies. However, they can form products via nonadiabatic transitions to the $^2\Sigma_{1/2}$ state. The two states of $^2A'$ symmetry are electronically coupled with each other and form a conical intersection [10]. Thus, two types of nonadiabatic coupling (i) Σ–Π electronic coupling and (ii) Σ–Π and Π–Π relativistic SO coupling, govern the nuclear dynamics following photodetachment. Recently, Capecchi and Werner have carried out multireference configuration interaction calculation and developed multiparameter global fits to calculate accurate potential energy surfaces for the above mentioned three electronic states and three nonadiabatic coupling surfaces between them [11]. We used these PESs in dynamical simulations presented here.

In the theoretical simulations the eigenfunctions of the energy levels of the electronic ground state of Cl^-–HD are vertically promoted to the coupled manifold of Cl···HD electronic states. These are then propagated on this final electronic manifold by numerically solving the time-dependent Schrödinger (TDSE) equation. The anionic wavefunctions are calculated by spectral quantization algorithm [12]. The channel specific dissociation probabilities of Cl···HD are calculated by recording the dissociative flux of the wave packet (WP) in time. We find that the nuclear dynamics is significantly affected by the nonadiabatic interactions. For instance, when the initial wavefunction is prepared on the $^2\Sigma_{1/2}$ electronic state, more WP flux moves to the reactive channels HCl + D or DCl + H in the coupled states situation than in the uncoupled one. The reactivity of the $^2\Pi_{3/2}$ and $^2\Pi_{1/2}$ electronic states via nonadiabatic transition to the $^2\Sigma_{1/2}$ state mostly populates the Cl + HD non-reactive channel of the latter. The dissociation to the reactive channels of the $^2\Sigma_{1/2}$ state in these cases are far less compared to the situation when dynamics is initiated on the $^2\Sigma_{1/2}$ electronic state. The formation of HCl + D is found to be more than DCl + H also for the excited eigenlevels of Cl^-–HD.

The theoretical computational details to treat the nuclear dynamics in the coupled manifold of electronic states are described in Section 2. In Section 3, we present the quantum dynamical results and discuss them. Finally, the paper is closed with a brief summary in Section 4.

2. Theoretical and computational details

The Cl^-–HD anion is promoted to the reactive PES of neutral Cl···HD upon photodetachment. A Franck–Condon (FC) transition is assumed for this step and the subsequent reactive dynamics of Cl···HD is simulated by means of quantum WP propagation. The final products (in their electronic ground state) may emerge in one of the following three channels, viz., (a) HCl + D (R1), (b) DCl + H (R2) and (c) Cl + HD (NR). Here R1 and R2 represents the two reactive channels and 'NR' stands for the non-reactive channel. The channel specific dissociation probabilities are calculated both for the uncoupled and coupled surface situations for the $^2\Sigma_{1/2}$ electronic state. Since, the $^2\Pi_{3/2}$ and $^2\Pi_{1/2}$ electronic states yield products in their electronic ground state via nonadiabatic transitions to the $^2\Sigma_{1/2}$ state, the dynamics of these states are simulated in the coupled surface situation only. All dynamical calculations are carried out for the lowest value of the total angular momentum; $J = 0$ and 0.5 in the nonrelativistic and relativistic situations, respectively, and the effect of excited vibronic levels of Cl^-–HD on the nuclear dynamics is examined. The WP propagation in the coupled electronic manifold is carried out in a diabatic electronic representation [13]. This is to avoid the singular derivative coupling terms of the adiabatic electronic representation [14]. However, the latter representation is more realistic and therefore, the adiabatic initial WP pertinent to the Cl^-–HD anion transformed to a diabatic electronic basis prior to its propagation on the Cl···HD electronic states and the time-evolved WP at each time is transformed back to the adiabatic electronic basis again to calculate the dynamical quantities.

2.1. The Hamiltonian

The nuclear dynamics is simulated here on the three lowest electronic states of Cl···HD including both the electronic and SO couplings among them. We use Jacobi coordinates R (distance between Cl and the center of mass of HD diatom), r (HD internuclear distance) and γ (the angle between $\vec{R}$ and $\vec{r}$) in the body-fixed frame in the dynamical simulations. The body-fixed z axis is defined to be parallel to R and the diatom is in the (x, z) plane. The various angular momentum operators and their corresponding projection quantum numbers are defined following the work of Rebentrost and Lester [15], Schatz et al. [16] and Alexander et al. [17]. They are listed in Table 1. With this set of coordinates, the Hamiltonian of Cl···HD system for total angular momentum $J \neq 0$ in a diabatic electronic basis can be expressed as

$$\mathcal{H} = \mathcal{H}^{\mathrm{Nu}}\mathbf{1} + \mathcal{H}^{\mathrm{el}} + \mathcal{H}^{\mathrm{so}} \quad (1)$$

Table 1
Description of various angular momentum terms used in the Hamiltoninan

Symbol	Description
$\boldsymbol{l}$	Electronic orbital angular momentum
$\boldsymbol{s}$	Electronic spin angular momentum
$\boldsymbol{L}$ ($=\boldsymbol{l}+\boldsymbol{s}$)	Total electronic angular momentum
$\boldsymbol{j}$	Nuclear rotational angular momentum of the diatom
$\boldsymbol{N}$	Nuclear orbital angular momentum of the atom realtive to the diatom
$\boldsymbol{J}$ ($=\boldsymbol{L}+\boldsymbol{j}+\boldsymbol{N}$)	Total (electronic + nuclear) angular momentum

where $\mathcal{H}^{\mathrm{Nu}}$ is the (diagonal) nuclear Hamiltonian matrix. The elements of which can be expressed as

$$\mathcal{H}^{\mathrm{Nu}} = -\frac{\hbar^2}{2\mu}\frac{\partial^2}{\partial R^2} - \frac{\hbar^2}{2\mu'}\frac{\partial^2}{\partial r^2} - \frac{\hbar^2}{2I}\frac{1}{\sin\gamma}\frac{\partial}{\partial\gamma}\left(\sin\gamma\frac{\partial}{\partial\gamma}\right) + \frac{\boldsymbol{J}^2+\boldsymbol{L}^2}{2\mu R^2} - \frac{2\boldsymbol{J}\cdot\boldsymbol{L}+2\boldsymbol{J}\cdot\boldsymbol{j}-2\boldsymbol{j}\cdot\boldsymbol{L}}{2\mu R^2}. \quad (2)$$

The first two terms in the right hand side of the above equation represent the radial kinetic energy operators along R and r, respectively. The quantity, $\mu = m_{\mathrm{Cl}}(m_{\mathrm{H}}+m_{\mathrm{D}})/(m_{\mathrm{Cl}}+m_{\mathrm{H}}+m_{\mathrm{D}})$ is the (Cl, HD) reduced mass, $\mu' = m_{\mathrm{H}}m_{\mathrm{D}}/(m_{\mathrm{H}}+m_{\mathrm{D}})$, is the HD reduced mass and m_{Cl}, m_{H} and m_{D} are the masses of Cl, H and D nuclei, respectively. The quantity I represents the moments of inertia of the collisional system,

$$\frac{1}{I} = \frac{1}{\mu R^2} + \frac{1}{\mu' r^2}.$$

In Eq. (1), $\mathcal{H}^{\mathrm{el}}$ represents the nonrelativistic electronic Hamiltonian matrix and $\mathcal{H}^{\mathrm{so}}$ is the relativistic SO Hamiltonian matrix. In a diabatic electronic basis the matrix representation of $\mathcal{H}^{\mathrm{el}} + \mathcal{H}^{\mathrm{so}}$ is non-diagonal. The various off-diagonal terms of this matrix represent the nonadiabatic coupling between the participating electronic states. By following the prescription of Alexander et al. [17], $\mathcal{H}^{\mathrm{el}} + \mathcal{H}^{\mathrm{so}}$ for the $^2\Sigma_{1/2}$, $^2\Pi_{3/2}$ and $^2\Pi_{1/2}$ electronic states of Cl···HD (1A′, 1A″ and 2A′ species, respectively, at the non-collinear geometry) is given by

$$\mathcal{H}^{\mathrm{el}} + \mathcal{H}^{\mathrm{so}} = \begin{pmatrix} V_\Sigma & -V_1 - i\sqrt{2}B & V_1 \\ -V_1 + i\sqrt{2}B & V_\Pi + A & V_2 \\ V_1 & V_2 & V_\Pi - A \end{pmatrix}, \quad (3)$$

where V_1 represents the Σ–Π electronic coupling, $A = i\langle\Pi_y|\mathcal{H}^{\mathrm{so}}|\Pi_x\rangle$, and, $B = \langle\bar{\Pi}_x|\mathcal{H}^{\mathrm{so}}|\Sigma\rangle$ are the components of the Π–Π and Σ–Π SO coupling Hamiltonian. The elements of the above Hamiltonian matrix are calculated by Capecchi and Werner [11] employing the state-of-the-art ab initio methods. We use this PESs for our dynamical calculations presented below.

2.2. Preparation of initial wavefunction

The initial wavefunctions corresponding to the anionic precursor are obtained by calculating the eigenenergy levels of its electronic ground state. The ab initio PES reported by Alexander [18] is employed for the latter. The spectral quantization algorithm [12] is utilized to calculate the eigenvalues and eigenfunctions of the bound energy levels supported by this PES. In this approach a set of pseudo-spectra is generated by propagating suitable Gaussian WPs on this PES. The time autocorrelation function is recorded and Fourier transformed to the energy domain to generate the pseudo-spectrum. The spectral intensity is given by

$$I(E) \int \langle\Psi(0)|\mathrm{e}^{-iHt/\hbar}|\Psi(0)\rangle\,\mathrm{e}^{iEt/\hbar}\,\mathrm{d}t, \quad (4)$$

where the first term in the integral kernel represents time autocorrelation function and is calculated by solving the (TDSE): $i\hbar(\partial\Psi/\partial t) = H\Psi$. The quantity H represents the Hamiltonian operator of Cl^-–HD anion. Energy values corresponding to the maximum intensities in the spectrum represent the eigenvalues of the energy levels of the anionic PES. The eigenfunctions are then obtained by projecting a time-evolved WP onto the desired eigenlevel (E_n) as

$$\Psi_n(R, r, \gamma, E) = \int_0^T \Psi(R, r, \gamma, t)\,\mathrm{e}^{iE_nt/\hbar}\,\mathrm{d}t. \quad (5)$$

In computing the eigenfunctions using Eq. (5), the wave packet is time evolved sufficiently long (up to 555 fs) in order to obtain the converge results. This convergence is further confirmed below while discussing the dissociation probability results.

The pseudo-spectrum obtained by initially locating a GWP near the equilibrium geometry of Cl^-–HD is shown in Fig. 1. The peaks in Fig. 1 correspond to the bound states supported in the potential well (∼0.12 eV deep) of Cl^-–HD anion. The energy corresponding to the maximum of each peak in the spectrum is obtained by fitting the latter to a Lorentzian line-shape function. The eigenfunctions are calculated by equation [5] and are averaged over r coordinate and plotted in Fig. 2(a–g) in terms of their probability density ($|\Psi|^2$) contours in the (γ, R) plane. These are assigned in terms of the number of nodes along R, r and γ coordinates and these are also indicated in the respective panel. In the Cl^-–HD PES two minima occurring for the linear $Cl^-\cdots$HD and $Cl^-\cdots$DH configurations, respectively, are separated by a barrier of ∼800 cm^{-1} at the T-shaped geometry [19]. Therefore, both the regions of the PES near $\gamma = 0$ and Π are populated due to quantum mechanical tunneling and can be seen from the wavefunction plots in Fig. 2(a–g).

The adiabatic initial wavefunctions of the anion presented above are subjected to FC transition to the adiabatic electronic states of the neutral species. They are then transformed to a diabatic electronic basis by, $\Psi^{\mathrm{d}} = S\Psi^{\mathrm{ad}}$, where S is the adiabatic-to-diabatic transformation matrix. The latter represents the eigenvector matrix which diagonalizes $\mathcal{H}^{\mathrm{el}} + \mathcal{H}^{\mathrm{so}}$. This matrix is numerically diagonalized at each node of the grid constructed here for the propagation of the WP and the transformation of the wavefunction between the adiabatic and diabatic electronic representations is carried out accordingly.

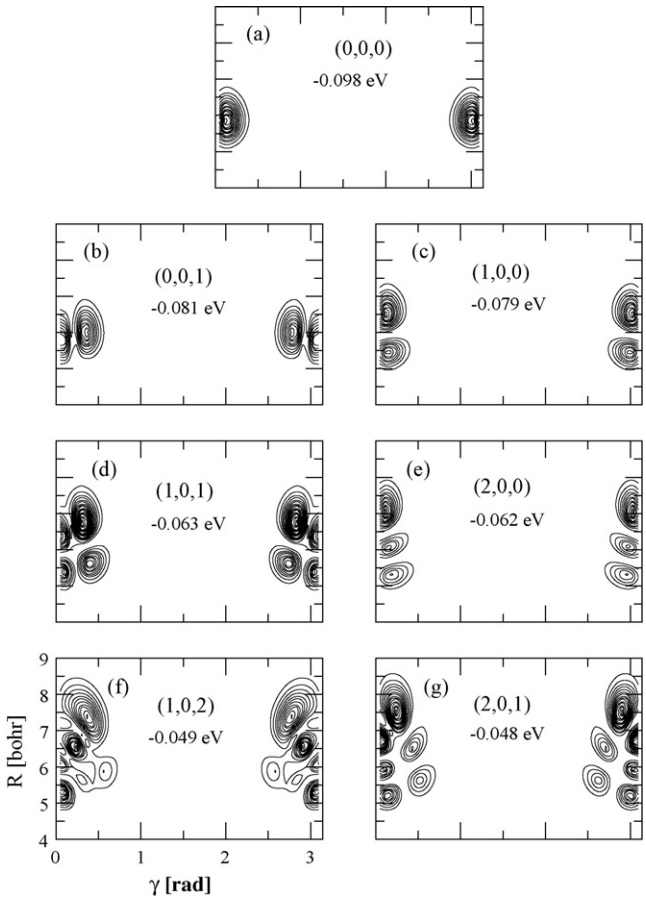

Fig. 2. The probability density contours of the eigenfunctions of the energy levels of the electronic ground state of the Cl^-–HD anion. These are calculated by the spectral quantization algorithm (see text) and plotted in the (γ, R) plane. The eigenfunctions are averaged over r. The energy eigenvalue and the assignment in terms of number of nodes along R, r and γ are given for each eigenstate in the respective panel.

2.3. Wave packet propagation and dissociation probability

The initial WP discussed above is propagated in the coupled manifold of the final diabatic electronic states with the aid of the TDSE, $|\Psi(t)\rangle = \exp[-i\mathcal{H}t/\hbar]\Psi(t=0)$. The TDSE is numerically solved on a grid consisting of equally spaced points along the Jacobi distances R (128 points in the range $1.0a_0$ to $14.0a_0$) and r (64 points in the range $0.1a_0$ to $8.0a_0$). The grid along γ is chosen as the nodes of a 49-points Gauss–Legendre quadrature [20]. The calculations are carried out for the lowest value of the total angular momentum ($J=0.5$ with and $J=0$ without the SO coupling). The Coriolis coupling terms of the Hamiltonian are not included in the present calculations.

The exponential time evolution operator in the TDSE (see above) at each time step is evaluated by the second-order split-operator method [21]. The fast Fourier transform method [22] and the discrete variable representation method [23] are used to evaluate the action of the radial and angular kinetic energy operators on the wave functions, respectively. In order to avoid the unphysical reflections of the fast moving components of the WP at the grid boundaries a sine-type of damping potential [24] is activated at the last 32 grid points along R and the last 15 grid points along r. The WP is propagated in time with a step size of $\Delta t \sim 0.13$ fs for a total propagation time of ~ 550 fs. The convergence of the results is explicitly checked by varying all the grid parameters noted above.

In order to access the energy distribution, we calculate the time autocorrelation function of the wave packet, $\langle\Psi(0)|\Psi(t)\rangle$, evolving on the neutral electronic states upon photodetachment. A Fourier transform of this autocorrelation function yields the photodetachment spectrum (cross-sections), revealing the range of energy covered by the initial wave packet. For illustration, a photodetachment spectrum obtained with (0, 0, 0) anionic wavefunction evolving on the $^2\Sigma_{1/2}$ adiabatic electronic state of ClHD is shown in Fig. 3.

The time-evolved WP at each time t is transformed back to the adiabatic electronic representation by using the hermitian conjugate of the S matrix and its asymptotic components on the $^2\Sigma_{1/2}$ electronic state are analyzed to calculate the dissociation probabilities. Only the components on the $^2\Sigma_{1/2}$ electronic state are of interest here because, as stated above, the components on the $^2\Pi_{3/2}$ and $^2\Pi_{1/2}$ electronic states do not yield products in their electronic ground state. However, we note that the NR components on the latter states are examined also in order to check the convergence of the dissociation probability results. The initial state-selected and time-resolved dissociation probabilities are obtained by integrating the WP flux at a dividing surface at, $r=r_d$ (located far out in the desired channel) as

$$P_i(t) = \langle\Phi(R, r, \gamma, t)|\hat{F}|\Phi(R, r, \gamma, t)\rangle|_{r=r_d} \quad (6)$$

where $P_i(t)$ is the dissociation probability starting form an initial state i of Cl^-–HD and averaged over all final states of the dissociative fragments of Cl···HD. The flux operator $\hat{F}$ in terms of a specific channel coordinate (say, r) is given by

$$\hat{F} = -\frac{i\hbar}{2\mu}\left[\frac{\partial}{\partial r}\delta(r-r_d) + \delta(r-r_d)\frac{\partial}{\partial r}\right]. \quad (7)$$

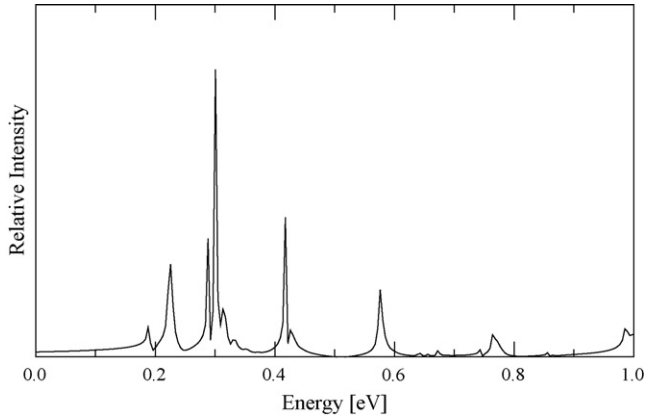

Fig. 3. The photodetachment spectrum of $ClHD^-$ for a transition of the initial (0, 0, 0) to the uncoupled $^2\Sigma_{1/2}$ adiabatic SO states of $Cl(^2P)$ + HD. The intensity in arbitrary units is plotted as a function of the energy of the final electronic state E. The zero of the energy scale corresponds to the asymptotically separated Cl + HD on the $^2\Sigma_{1/2}$ state.

With this, the dissociation probability in Eq. [6] assumes the form

$$P_i(t) = \frac{\hbar}{\mu}\mathrm{Im}\left[\left\langle \Phi(R, r_\mathrm{d}, \gamma, t) \left| \frac{\partial\Phi(R, r_\mathrm{d}, \gamma, t)}{\partial r} \right\rangle\right]_{r=r_\mathrm{d}}. \quad (8)$$

The quantity in the right-hand side is integrated over the whole range of R and γ to obtain the dissociation probability at each time t which is further integrated over t to calculate the total dissociation probability. Here we note that the distinction between the two reactive channels (R1 and R2) in the product asymptote is made by comparing the internuclear distances of the product HCl and DCl molecules. The reactive flux [Eq. (7)], in which the HCl distance is smaller than the DCl distance is considered to represent the (R1) channel and the rest is considered to represent the (R2) channel.

3. Results and discussion

In order to clearly revel the effects of nonadiabatic coupling on the Cl···HD dissociation dynamics, we first consider the FC transition of the (0, 0, 0) wavefunction of Cl^-–HD (cf., Fig. 2(a)) to the uncoupled adiabatic $^2\Sigma_{1/2}$ electronic state of the neutral Cl···HD. The equilibrium geometry of the Cl^-–HD anion is significantly stretched along R ($\sim 6a_0$). Therefore, the FC transition promotes this anionic wavefunction to the van der Waals well region of the reagent asymptote of the reactive Cl···HD PES. This well has a depth of ~0.51 kcal/mol and occurs for $R = 5.78a_0$, $r = 1.403a_0$ and $\gamma = 90°$ and is sufficiently away from the barrier (hight~7.88 kcal/mol) region of the potential energy surface occurring at $R = 3.631a_0$, $r = 1.854a_0$ and $\gamma = 0°$ [10,11]. The resulting time-dependent dissociation probabilities for the R1, R2 and NR channels are plotted in Fig. 4 and are indicated by different line types in the panel. The total dissociation probabilities (integrated over time) are shown as a bar diagram in the inset. In the latter, the results from the initial wavefunctions calculated by the spectral quantization scheme (as discussed above) and also by a relaxation scheme [25] using the Lanczos propagator are shown (indicated by a and b, respectively, in the inset). The identity of the two results revel the convergence of the initial wavefunctions calculated here by the spectral quantization method. It can be seen from Fig. 4 that dissociation to the Cl + HD (NR) channel is dominated followed by the HCl + D (R1) channel on the uncoupled $^2\Sigma_{1/2}$ electronic state. Also the R1 channel dominates over the DCl + H (R2) channel in the dynamics.

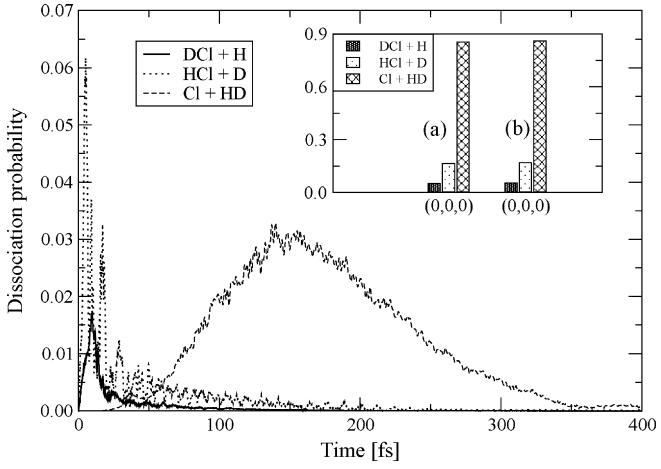

Fig. 4. Time-dependent dissociation probabilities of Cl···HD to the DCl + H (solid line), HCl + D (dotted line) and Cl + HD (dashed line) channels of the $^2\Sigma_{1/2}$ electronic state. The Cl···HD species is prepared by photodetaching Cl^-–HD from the (0, 0, 0) level of its electronic ground state. This initial wavefunction is evolved on the uncoupled $^2\Sigma_{1/2}$ electronic state of the neutral to calculate the dissociation probabilities. The total dissociation probabilities (integrated over time) of the three channels obtained by using the initial wavefunction calculated by (a) a relaxation scheme and (b) the spectral quantization method are shown in the inset.

Based on a statistical argument, the DCl yield is expected to be more than the HCl yield. This is found to be the case in bimolecular Cl(^{2}P) + HD scattering calculations. However, this does not seem to be the case for the unimolecular dissociation of the Cl···HD complex treated here. Moreover, the initial wave packet here is located at the van der Waals well region of the reagent asymptote rather than far out in the reagent channel as in a bimolecular collision. The nuclear dynamics followed by the initial FC transition of the above (0, 0, 0) anionic wavefunction separately to the $^2\Sigma_{1/2}$, $^2\Pi_{3/2}$ and $^2\Pi_{1/2}$ adiabatic electronic states of the neutral Cl···HD in the coupled states situation is considered next. Both the electronic and relativistic SO coupling are activated in the dynamical simulations. The results are presented in Fig. 5(a–c), respectively. The adiabatic initial anionic wavefunction is transformed to diabatic electronic basis and propagated in the coupled manifold of the electronic states (cf., Hamiltonian in Eq. (1)) of neutral Cl···HD. In Fig. 5(a), the anionic wavefunction is initially promoted to the $^2\Sigma_{1/2}$ electronic state of the neutral. It can be seen form Fig. 5(a) that the reactive R1 channel still dominates over the R2 channel of the $^2\Sigma_{1/2}$ adiabatic electronic state and the dissociation to its NR channel is significantly less than what was observed in the uncoupled surface situation (cf., Fig. 4). It can be seen also that dissociation to both the reactive channel also increases in the coupled surface situation. Therefore, the nonadiabatic coupling enhances the reactive dissociation and reduces the non-reactive dissociation of Cl···HD. We note here that the sum of total dissociation probabilities on the $^2\Sigma_{1/2}$ state shown in the inset of Fig. 5(a) is less than 1.0 and is only ~0.69. The remaining of the WP dissociates in the NR channel of the $^2\Pi_{3/2}$ and $^2\Pi_{1/2}$ electronic states and are also indicated in the inset.

The reactivity of the $^2\Pi_{3/2}$ electronic state via nonadiabatic transitions to the $^2\Sigma_{1/2}$ electronic state is shown in Fig. 5(b). The (0, 0, 0) anionic wavefunction in this case is promoted to the $^2\Pi_{3/2}$ adiabatic electronic state of the neutral initially, and evolved in the coupled diabatic electronic manifold of the latter. In this case, as can be seen from the inset, the dissociation to the NR channel of the $^2\Sigma_{1/2}$ electronic state dominates. The dissociation to the reactive R1 channel and R2 channels is practically insignificant. The remaining of the WP dissociates to the NR channel of $^2\Pi_{3/2}$ and $^2\Pi_{1/2}$ electronic states. Therefore, it can be concluded that the nonadiabatic transition of the WP (prepared initially on the $^2\Pi_{3/2}$ state) to the $^2\Sigma_{1/2}$ state leads to the dissociation predominately via the NR channel of the latter. The same scenario as in the case of Fig. 5(b) persists for an initial

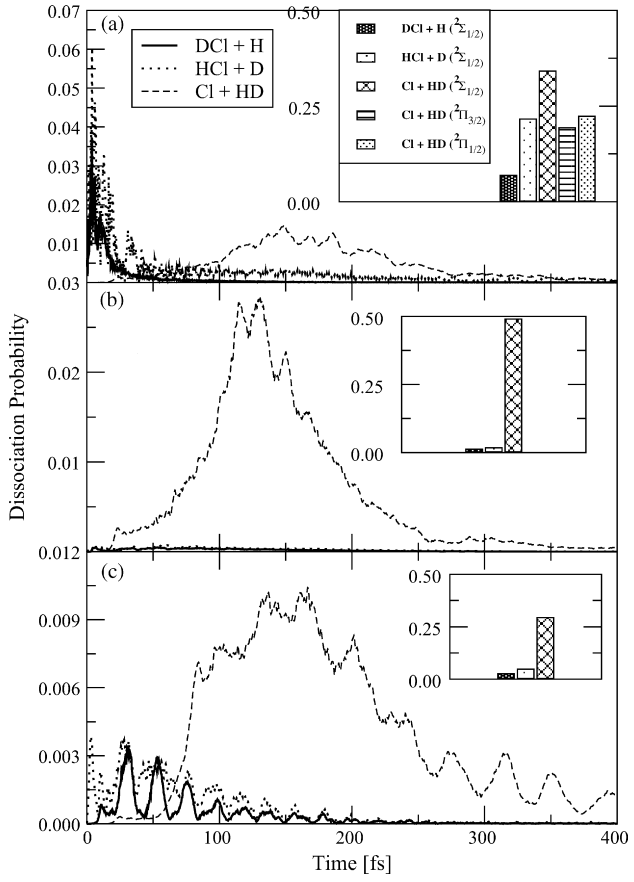

Fig. 5. Same as in Fig. 3, obtained for the transition of the (0, 0, 0) wavefunction of the Cl^-–HD anion to the (a) $^2\Sigma_{1/2}$, (b) $^2\Pi_{3/2}$ and (c) $^2\Pi_{1/2}$ adiabatic electronic state of Cl···HD. The nuclear dynamics in each case is simulated in the coupled (both electronic and SO) manifold of electronic states of the latter. The total dissociation probabilities to the non-reactive channels of the excited $^2\Pi_{3/2}$ and $^2\Pi_{1/2}$ states are also included in the inset of panel (a).

transition of the (0, 0, 0) anionic wavefunction to the $^2\Pi_{1/2}$ electronic state of Cl···HD and is depicted in Fig. 5(c). However, in this case the dissociation probabilities to the reactive R1 and R2 channels of the $^2\Sigma_{1/2}$ state are somewhat larger than those observed in Fig. 5(b). Here also the remaining of the WP dissociates to the NR channels of the $^2\Pi_{3/2}$ and $^2\Pi_{1/2}$ electronic states. The results presented in Fig. 5(a–c) reveal that the products are formed in their electronic ground state with better yield when the dynamics is initiated on the $^2\Sigma_{1/2}$ electronic state of Cl···HD.

In order to better understand the above quantum dynamical results, we show in Fig. 6(a–c) the time-dependence of the adiabatic electronic populations in the coupled state dynamics of Cl···HD. The results of the initial FC transition of Cl^-–HD to the adiabatic $^2\Sigma_{1/2}$, $^2\Pi_{3/2}$ and $^2\Pi_{1/2}$ electronic states of Cl···HD are shown in the panel a, b and c, respectively. These adiabatic initial wavefunctions are evolved in the coupled manifold of the diabatic electronic states of Cl···HD and adiabatic electronic populations are calculated at each time t. In each panel the electronic populations of the three states are indicated by different line types. These represent fractional populations. Since the initial wavefunction in Fig. 6(a) is initially located on the $^2\Sigma_{1/2}$ adiabatic electronic state its population is 1.0 at $t = 0$. The populations of the $^2\Pi_{3/2}$ and $^2\Pi_{1/2}$ are therefore zero initially. At later times the WP on the $^2\Sigma_{1/2}$ electronic state reaches the Σ–Π curve crossing regions and population transfer to the $^2\Pi_{3/2}$ and $^2\Pi_{1/2}$ adiabatic electronic states takes place. This is indicated by a decrease in the $^2\Sigma_{1/2}$ and a growth in the $^2\Pi_{3/2}$ and $^2\Pi_{1/2}$ electronic populations. The population of the $^2\Sigma_{1/2}$ electronic state sharply decreases to ∼58% within ∼20 fs followed by quasiperiodic recurrences. It can be seen from Fig. 6(a) that somewhat more population transfer takes place to the $^2\Pi_{1/2}$ electronic state when compared to that to the $^2\Pi_{3/2}$ electronic state. For instance, ∼30% of the WP moves to the $^2\Pi_{1/2}$ and only ∼12% to the $^2\Pi_{3/2}$ electronic state at ∼20 fs. The oscillations in the population curves indicates the transfer of the WP back and forth through the curve crossings of different electronic states.

The population curves for an initial transition of the anion to the $^2\Pi_{3/2}$ state of the neutral are plotted in Fig. 6(b). In this case the decay of the $^2\Pi_{3/2}$ electronic population is not as large as that observed for the $^2\Sigma_{1/2}$ state in panel a. The population transfer to the $^2\Sigma_{1/2}$ state (solid line) is more than that to the $^2\Pi_{1/2}$ state (dashed line). However, it seems that the major fraction of the WP dissociates to the NR channel of the $^2\Pi_{3/2}$ electronic state leading to Cl + HD.

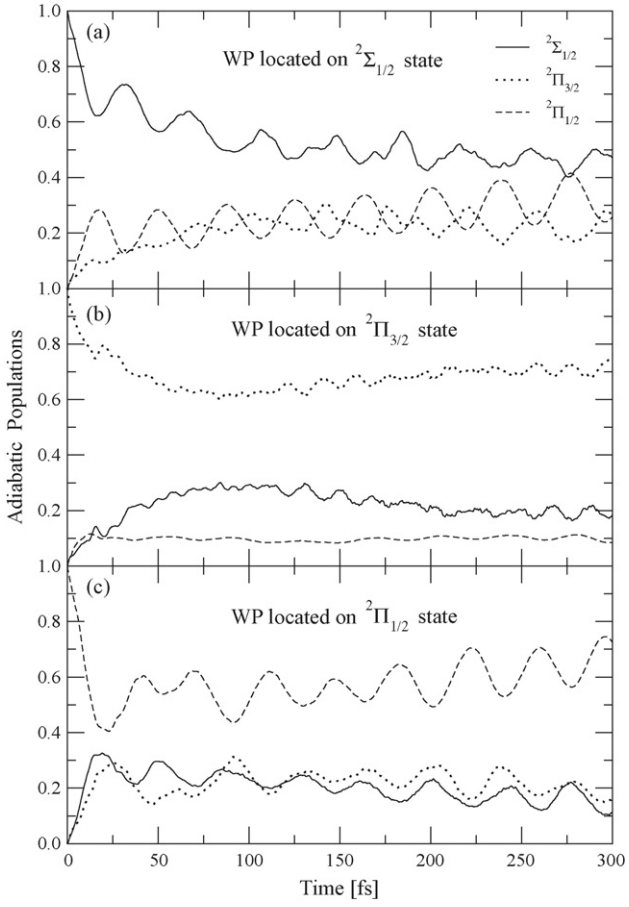

Fig. 6. Time dependence of the adiabatic electronic populations in the coupled state dynamics of Fig. 5. The initial WP in panel a, b and c corresponds to that of panel a, b and c, respectively, of Fig. 5. The populations of the $^2\Sigma_{1/2}$, $^2\Pi_{3/2}$ and $^2\Pi_{1/2}$ adiabatic electronic states in each panel are shown by the solid, dotted and dashed lines.

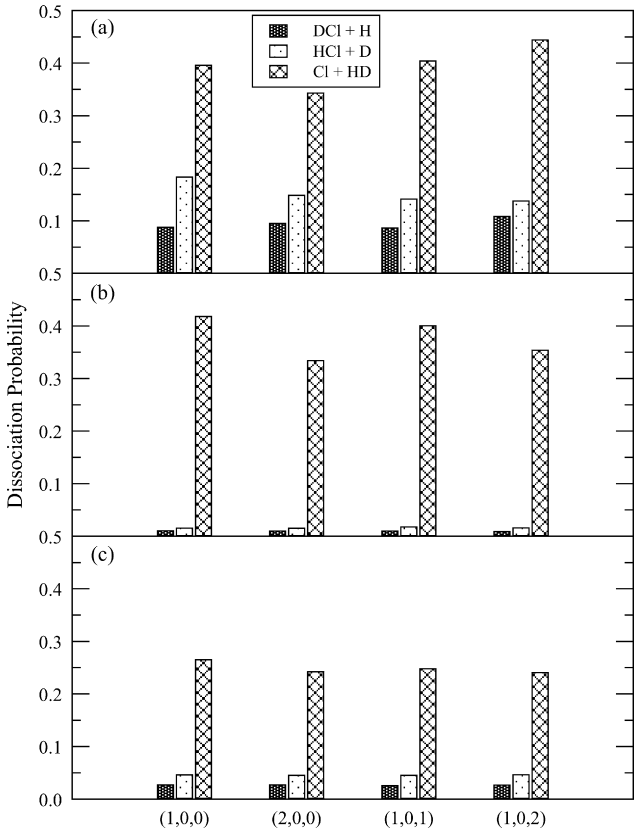

Fig. 7. The time-integrated total dissociation probabilities of internally excited eigenlevels of Cl^-–HD to the HCl + D, DCl + H and Cl + HD channels of the $^2\Sigma_{1/2}$ electronic state of Cl···HD. The results obtained from the initial FC transition of the anion to the $^2\Sigma_{1/2}$, $^2\Pi_{3/2}$ and $^2\Pi_{1/2}$ electronic state of the neutral are shown in panel a, b and c, respectively.

The scenario for an initial transition of the anion to the $^2\Pi_{1/2}$ electronic state of the neutral is depicted in Fig. 6(c). In contrast to the dynamics on the $^2\Pi_{3/2}$ electronic state, the nuclear motion on the $^2\Pi_{1/2}$ electronic state is much perturbed by the nonadiabatic interactions. As a result, relatively more fraction of the WP (as compared to panel b) moves to the $^2\Sigma_{1/2}$ and $^2\Pi_{3/2}$ electronic states. This also accounts for a relatively increased reactive dissociation of Cl···HD on the $^2\Sigma_{1/2}$ electronic state (cf. Fig. 5(b) versus Fig. 5(c)) for this initial condition.

In Fig. 7(a–c) we show the dissociative photodetachment dynamics of the excited eigen levels of the ground electronic state of Cl^-–HD. We plot the time-accumulated dissociation probabilities for these initial wavefunctions promoted to the $^2\Sigma_{1/2}$, $^2\Pi_{3/2}$ and $^2\Pi_{1/2}$ adiabatic electronic states of Cl···HD, respectively, in panel a, b and c. It can be seen that the dissociation to the DCl + H channel increases and to the HCl + D channel decreases upon internal excitation. However, no significant change in the dissociation probabilities can be observed for the initial transition to the $^2\Pi_{3/2}$ and $^2\Pi_{1/2}$ electronic states of Cl···HD. In all cases the NR channel dominates and HCl + D formation is preferred over DCl + H formation. As stated before that the initial wavefunction corresponding to the anion is a vibrationally averaged one, and therefore, the dependence of the dissociation probability results on the initial vibrational excitation of the anion in the present situation cannot be inferred.

4. Summary

We presented a brief theoretical account of the dissociative photodetachment dynamics of Cl^-–HD anion. Photodetachment of Cl^-–HD anion prepares the neutral Cl···HD species in the van der Waals well region of the reagent (Cl + HD) asymptote of its reactive PES. The latter represents a manifold of three electronic states coupled by the electronic and relativistic SO interactions. The dissociation of Cl···HD complex occurs on its lowest $^2\Sigma_{1/2}$ electronic states and the products emerge in their electronic ground state in three different R1, R2 and NR channels. The $^2\Pi_{3/2}$ and $^2\Pi_{1/2}$ electronic state of Cl···HD can form the dissociative fragments in their electronic ground state only by non-Born–Oppenheimer transition to the $^2\Sigma_{1/2}$ state.

The eigenfunctions of the vibronic levels of Cl^-–HD anion are calculated and are vertically promoted to the coupled manifold of electronic states of Cl···HD. The dissociation of the latter subsequently monitored by a time-dependent WP propagation approach. The nonadiabatic coupling is observed to enhance the reactivity of the $^2\Sigma_{1/2}$ electronic state. Generally, for all initial transitions to the $^2\Sigma_{1/2}$, $^2\Pi_{3/2}$ or $^2\Pi_{1/2}$ electronic states of Cl···HD and for internally excited initial wavefunctions of the anion the reactive HCl + D channel dominates over the DCl + H channel. The dissociation to the NR channel is always more than the rest. The effect of the nonadiabatic coupling on the nuclear dynamics on the $^2\Pi_{1/2}$ electronic state appears to be significantly more that that on the $^2\Sigma_{1/2}$ and $^2\Pi_{3/2}$ electronic states of Cl···HD. Finally, we mention that the photodetachment recording on Cl^-–HD anion has been carried out and it will be worthwhile to extend these measurements with the aid of photofragment translational spectroscopy in order to validate the accuracy of the PESs and the theoretical findings of the present article.

Acknowledgments

This study is in part supported by a research grant from the Council of Scientific and Industrial Research (Grant No. CSIR-01(1917)/04/EMR-11). S.G. acknowledges University Grants Commission (UGC), New Delhi for the Senior Research Fellowship. We also thank UGC and the department of Science and Technology, New Delhi, for the Computational facilities provided under the UPE and HPCF programs, respectively, in the University of Hyderabad.

References

[1] (a) A. Stolow, A.E. Bragg, D.M. Neumark, Chem. Rev. 104 (2004) 1719;
(b) D.M. Neumark, Annu. Rev. Phys. Chem. 52 (2001) 255;
D.M. Neumark, Science 272 (1997) 1446;
D.M. Neumark, Acc. Chem. Res. 26 (1993) 33.
[2] P.G. Wenthold, C. Lineberger, Acc. Chem. Res. 32 (1999) 597.
[3] R.E. Continetti, Int. Rev. Phys. Chem. 17 (1998) 227;
R.E. Continetti, Annu. Rev. Phys. Chem. 52 (2001) 165.
[4] (a) H.-J. Deyerl, T.G. Clements, A.K. Luong, R.E. Continetti, J. Chem. Phys. 115 (2001) 6931;
(b) K.A. Hanold, M.C. Garner, R.E. Continetti, Phys. Rev. Lett. 77 (1996) 3335;

(c) T.G. Clements, H.-J. Deyerl, R.E. Continetti, J. Phys. Chem. A 106 (2002) 279;
(d) Z. Lu, R.E. Continetti, J. Phys. Chem. A 108 (2004) 9962.
[5] T.G. Clements, R.E. Continetti, J.S. Francisco, J. Chem. Phys. 117 (2002) 6478.
[6] (a) T.C. Allison, S.L. Mielke, D.W. Schwenke, G.C. Lynch, M.S. Gordon, D.G. Truhlar, in: H.-R. Volp, J. Wolfrum, R. Rannacher, J. Warnatz (Eds.), Gas-phase Reaction Systems: Experiments and Models 100 Years After Max Bodenstein, Springer, Heidelberg, 1996, p. 111;
(b) P. Casavecchia, Rep. Prog. Phys. 63 (2000) 355;
(c) M.H. Alexander, G. Capecchi, H.-J. Werner, Science 296 (2002) 715;
(d) S. Ghosal, S. Mahapatra, J. Chem. Phys. 121 (2004) 5740;
(e) M.H. Alexander, G. Capecchi, H.-J. Werner, Faraday Disc. 127 (2004) 59;
(f) D. Skouteris, D.E. Manolopoulos, W. Bian, H.-J. Werner, L.-H. Lai, K. Liu, Science 286 (1999) 1713;
(g) S.-H. Lee, K. Liu, J. Chem. Phys. 111 (1999) 6253;
(h) F. Dong, S.-H. Lee, K. Liu, J. Chem. Phys. 115 (2001) 1197.
[7] (a) M.J. Ferguson, G. Meloni, H. Gomez, D.M. Neumark, J. Chem. Phys. 117 (2002) 8181;
(b) A. Osterwalder, M.J. Nee, J. Zhou, D.M. Neumark, J. Chem. Phys. 121 (2004) 6317.
[8] S. Ghosal, S. Mahapatra, Chem. Phys. Lett. 394 (2004) 207.
[9] S. Ghosal, S. Mahapatra, J. Phys. Chem. A 109 (2005) 1530.
[10] W. Bian, H.-J. Werner, J. Chem. Phys. 112 (2000) 220.
[11] G. Capecchi, H.-J. Werner, Phys. Chem. Chem. Phys. 6 (2004) 4975.
[12] R.T. Skodje, R. Sadeghi, H. Köppel, J.L. Krause, J. Chem. Phys. 101 (1994) 1725.
[13] (a) W. Lichten, Phys. Rev. 164 (1967) 131;
(b) F.T. Smith, Phys. Rev. 179 (1969) 111;
(c) T.F. O'Malley, Adv. At. Mol. Phys. 7 (1971) 223.
[14] H. Köppel, W. Domcke, L.S. Cederbaum, Adv. Chem. Phys. 57 (1984) 59.
[15] F. Rebentrost, W.A. Lester Jr., J. Chem. Phys. 63 (1975) 3737;
F. Rebentrost, W.A. Lester Jr., J. Chem. Phys. 64 (1976) 3879;
F. Rebentrost, W.A. Lester Jr., J. Chem. Phys. 64 (1977) 4223.
[16] (a) G.C. Schatz, P. McCabe, J.N.L. Connor, Faraday Disc. 110 (1998) 139;
(b) T.W.J. Whiteley, A.J. Dobbyn, J.N.L. Connor, G.C. Schatz, Phys. Chem. Chem. Phys. 2 (2000) 549;
(c) G.C. Schatz, M. Hankel, T.W.J. Whiteley, J.N.L. Connor, J. Phys. Chem. A 107 (2003) 7278.
[17] M.H. Alexander, H.-J. Werner, D.E. Manolopoulos, J. Chem. Phys. 109 (1998) 5710;
M.H. Alexander, H.-J. Werner, D.E. Manolopoulos, J. Chem. Phys. 113 (2000) 11084.
[18] M.H. Alexander, J. Chem. Phys. 118 (2003) 9637.
[19] A.A. Buchachenko, T.A. Grinev, J. Klos, E.J. Bieske, M.M. Szcześniak, G. Chałasiński, J. Chem. Phys. 119 (2003) 12931.
[20] W.H. Press, B.P. Flannery, S.A. Teukolsky, W.T. Vatterling, Numerical Recipes: The Art of Scientific Computing, Cambridge University Press, Cambridge, England, 1986.
[21] M.D. Feit, J.A. Fleck Jr., A. Steiger, J. Comput. Phys. 47 (1982) 412.
[22] D. Kosloff, R. Kosloff, J. Comput. Phys. 52 (1983) 35.
[23] Z. Bačić, J.C. Light, Annu. Rev. Phys. Chem. 40 (1989) 469.
[24] S. Mahapatra, N. Satyamurthy, J. Chem. Soc. Faraday Trans. 93 (1997) 773.
[25] R. Kosloff, H. Tal-Ezer, Chem. Phys. Lett. 127 (1986) 223.